Check for updates

# Rationally tailored redox ability of Sn/γ-Al₂O₃ with Ag for enhancing the selective catalytic reduction of NOₓ with propene

Ning Li,[a] Tiantian Zhang,[b] Zuliang Wu,[bc] Jing Li,[bc] Wei Wang,[bc] Jiali Zhu,[bc] Shuiliang Yao*[bc] and Erhao Gao [ID] *[bc]

The development of excellent selective catalytic reduction (SCR) catalysts with hydrocarbons for lean-burn diesel engines is of great significance, and a range of novel catalysts loaded with Sn and Ag were studied in this work. It was found that the synergistic effects of Sn and Ag enabled the 1Sn5Ag/γ-Al₂O₃ (1 wt% Sn and 5wt% Ag) to exhibit superior $C_3H_6$-SCR performance. The de-NOₓ efficiency was maintained above 80% between 336 and 448 °C. The characterization results showed that the presence of AgCl crystallites in the 1Sn5Ag/γ-Al₂O₃ catalyst helped its redox ability maintain an appropriate level, which suppressed the over-oxidation of $C_3H_6$. Besides, the number of surface adsorbed oxygen ($O_\alpha$) and hydroxyl groups ($O_\gamma$) were enriched, and their reactivity was greatly enhanced due to the coexistence of Ag and Sn. The ratio of $Ag^0/Ag^+$ was increased to 3.68 due to the electron transfer effects, much higher than that of Ag/γ-Al₂O₃ (2.15). Lewis acid sites dominated the $C_3H_6$-SCR reaction over the 1Sn5Ag/γ-Al₂O₃ catalyst. The synergistic effects of Sn and Ag facilitated the formation of intermediates such as acetates, enolic species, and nitrates, and inhibited the deep oxidation of $C_3H_6$ into $CO_2$, and the $C_3H_6$-SCR mechanism was carefully proposed.

## 1. Introduction

Nitrogen oxides (NOₓ) are one of the main pollutants that cause atmospheric pollution such as acid rain, photochemical smog, and global warming, and cause serious harm to the ecological environment and human health.[1–3] Automotive exhaust is an important source of NOₓ emissions, of which diesel vehicle exhaust contributes around 90%. The large amount of NOₓ emissions has been one of the main reasons for the ozone pollution in many urban areas in China in recent years.[4] At present, the selective catalytic reduction technology (SCR) using NH₃ as a reducing agent has been commercially applied for diesel exhaust gas denitrification under lean-burn conditions.[5] However, NH₃-SCR technology requires addition of urea to generate ammonia, which increases operating costs, and NH₃ slip usually causes secondary pollution.

As an alternative, the technology of removing NOₓ by hydrocarbons (HCs) has attracted extensive attention, because no extra reducing agent needs to be supplemented, and the HC pollutants could be removed simultaneously. The saturated hydrocarbons would preferentially react with oxygen and showed poor activity, by contrast, the unsaturated hydrocarbons, such as propene could preferentially react with NOₓ under certain conditions.[6–8] However, $C_3H_6$-SCR technology generally has problems such as poor low-temperature activity and narrow temperature window, and the core of this problem lies in the design of catalysts. Optimizing the acidity and redox properties of the catalyst through bimetallic active components has been proved to be an effective method to improve the low-temperature de-NOₓ activity. More *et al.*[9] reported that Au adding onto Ag/Al₂O₃ effectively lowered the temperature window of $C_3H_6$-SCR, and the de-NOₓ efficiency reached nearly 100% at 350 °C. However, the high cost of the noble metals as active components restrains its application. Besides, it was also found that 7% Mg-doped Ag/Al₂O₃ could effectively improve the $C_3H_6$-SCR efficiency below 400 °C,[10] which suggests that the co-loading of noble metal and base metal is a feasible approach for $C_3H_6$-SCR activity promotion. The rational design of superior bi-metal supported catalysts for $C_3H_6$-SCR and the structure–performance relationships and reaction mechanism of the catalyst are worthy of being further explored.

Due to the abundant reserves and low price, transitional metal-based catalysts such as Cu, Sn, Fe, Co, and Mn have been widely studied for $C_3H_6$-SCR.[11–19] In addition, due to the strong oxidizing ability of precious metals and excellent NOₓ removal performance, Ag, Pt, Pd and other precious metals are also

*[a]School of Petrochemical Engineering, Changzhou University, Jiangsu, 213164, China*

*[b]School of Environmental Science and Engineering, Changzhou University, Jiangsu, 213164, China. E-mail: yaos@cczu.edu.cn*

*[c]Advanced Plasma Catalysis Engineering Laboratory for China Petrochemical Industry, Changzhou University, Jiangsu, 213164, China. E-mail: gaoerhao@cczu.edu.cn*

widely used in various industrial flue gases purification.[20,21] Among them, $SnO_2$ has been found to be rich in surface oxygen vacancies and acidic sites and showed great potential. Kung et al.[22] and Liu et al.[23] studied the $C_3H_6$-SCR performance of $SnO_2/Al_2O_3$ catalysts and found that the Sn loading has a significant effect on the de-$NO_x$ efficiency, and it reached a maximum value of 83% at 450 °C. Lai et al.[24] prepared a single-layer supported $SnO_2$/beta catalyst and the de-$NO_x$ efficiency reached 85% at 500 °C. It was found that the number of beneficial surface oxygen vacancies increased due to the electron transfer and interfacial interaction between $Sn^{4+}$ and H-beta support. Besides, Zhang et al.[11] studied the $C_3H_6$-SCR activity of $SnO_2$/ZSM-5 catalyst, which reached the highest de-$NO_x$ efficiency of ca. 80% at around 450 °C. The inferior catalytic activity in the low-temperature range is mainly due to its weak oxidation ability for $C_3H_6$, leading to its limited practical application. As one of the relatively cheap noble metals, supported Ag-based catalysts have also been extensively studied for $C_3H_6$-SCR. Chaieb et al.[25] and Wang et al.[26] studied the $C_3H_6$-SCR performance of $Ag/Al_2O_3$, and found that the de-$NO_x$ efficiency reached about 70% at 450 °C. He et al.[27,28] found that 4 wt% Ag loading amounts improved the de-$NO_x$ efficiency, reaching about 90% at 450 °C. However, unlike Sn-based catalysts, the main factor that restrains the SCR activity of Ag-based catalysts in the low-temperature range results from its strong oxidizing ability, which facilitates $C_3H_6$ to deeply oxidized into $CO_2$ instead of reactive organic intermediates to react with $NO_x$. Therefore, a combination of Sn and Ag is possibly conducive to a broadened temperature window. In addition, Wang et al.[29] reported that 2% $AgCl/Al_2O_3$ catalyst achieved almost 100% de-$NO_x$ efficiency between 300 and 500 °C with the reducing gases of $C_3H_6$ and $H_2$. They found that AgCl nanoparticles could promote the production of formats and enolic species. Due to the fact that the oxidation ability of AgCl nanoparticles was much weaker than that of $Ag_2O$, the presence of small amounts of AgCl particles might be conducive to suppressing the deep oxidation process of $C_3H_6$. Inspired by this, in addition to the preparation of Ag and Sn bimetallic supported catalysts, the present study will also introduce AgCl nanoparticles through using tin chloride salts to optimize the acidity and redox properties of the catalysts, thus further widening the low-temperature window of $C_3H_6$-SCR.

Herein, a series of $\gamma$-$Al_2O_3$ supported catalysts with different Sn/Ag ratios were prepared and their activity was tested in this work. Furthermore, the physicochemical properties of the catalysts were characterized by $N_2$ adsorption–desorption, scanning electron microscope (SEM), high resolution-transmission electron microscope (HR-TEM), X-ray diffraction (XRD), X-ray photoelectron spectroscopy (XPS), pyridine infrared (Py-IR), $H_2$-temperature programmed reduction ($H_2$-TPR), and $O_2$-temperature programmed desorption ($O_2$-TPD). Besides, in situ diffuse reflectance Fourier transform infrared spectroscopy (in situ DRIFTS) was carried out to explore the catalytic reaction mechanism. The structure–activity relationships of the $1Sn5Ag/\gamma$-$Al_2O_3$ catalyst and its $C_3H_6$-SCR mechanism were fully explored.

# 2. Experimental

## 2.1 Catalyst preparation

The catalysts tested in this work were prepared by wet impregnation method. As an example, $1Sn5Ag/\gamma$-$Al_2O_3$ catalyst was prepared as follows: an appropriate amount of fresh $\gamma$-$Al_2O_3$ was dried in an oven at 120 °C for 6 h and then calcined in a muffle furnace at 500 °C for 2 h for subsequent use. 0.0234 g $SnCl_4 \cdot 5H_2O$ and 888 µL standard $Ag(NO)_3$ solution (1.022 mol $L^{-1}$) were dissolved in 20 mL deionized water to prepare the impregnation solution, and then 1 g pre-treated $\gamma$-$Al_2O_3$ powder was add, and stir vigorously in a water bath at 80 °C for about 2 h until it is perfectly dry. The catalyst was then transferred into the oven and dried at 80 °C for 6 h. Finally, the catalyst was placed in a tube furnace and calcined at a temperature of 600 °C under air atmosphere for 6 h to obtain $1Sn/\gamma$-$Al_2O_3$. After that, a certain amount of $AgNO_3$ was dissolved in deionized water, then $1Sn/\gamma$-$Al_2O_3$ was dosed, and the above procedures were repeated to obtain the $1Sn5Ag/\gamma$-$Al_2O_3$ catalyst.

## 2.2 Catalyst characterization

$N_2$ adsorption–desorption was carried out with an automatic specific surface and porosity analysers (Micromeritics TriStar II 3020) at −196 °C. SEM was performed with a Zeiss SUPRA-55 field emission scanning electron microscope. HR-TEM was tested with the American FEI Talos F200S transmission electron microscope. XRD was measured using an X-ray diffractometer (Rigaku Ultima IV). The incident ray light source is a copper target, the test angle is 5–120°, and the step size is 0.02°. XPS was carried out with an X-ray photoelectron spectrometer (Thermo Scientific K-Alpha) equipment with monochromatic Al–K X-ray radiation at 250 W. $H_2$-TPR was carried out on the gas chromatography equipped with a thermal conductivity detector (TCD). 200 mg of the catalysts were placed in a U-type reaction tube, and the temperature was from room temperature to 300 °C at a ramp of 10 °C $min^{-1}$ under $O_2$ flow for 30 min to remove surface adsorbed species. Then 30 mL per min $N_2$ was purged for 30 min and cooled to 50 °C. The temperature was increased to 750 °C at a heating rate of 5 °C $min^{-1}$ in 5% $H_2/N_2$, and the signals were continuously recorded. $O_2$-TPD was also performed similarly. 200 mg of the catalysts were placed in a U-type reaction tube, and the temperature was from room temperature to 300 °C at a ramp of 10 °C $min^{-1}$ under $O_2$ flow for 30 min to remove surface adsorbed species. Subsequently, 30 mL per min $N_2$ was purged for 30 min to remove unstable surface adsorption of $O_2$ and cooled to 50 °C. Finally, the sample was heated from 30 °C to 600 °C at a rate of 5 °C $min^{-1}$ under an $N_2$ atmosphere. Py-IR and in situ DRIFTS were obtained on a Nicolet iS50 spectrometer equipped with in situ reaction cell (Harrick HVC-DRP-5), and the scan resolution was 4 $cm^{-1}$. After pretreatment in the Ar atmosphere at 400 °C for 1 h, the catalyst was reacted with pyridine vapor at 300 °C for 30 min, and the corresponding IR spectrum was recorded after stabilizing for 10 min. Prior to the in situ DRIFTS tests, the catalyst was pretreated in the in situ cell at 300 °C for 30 min under air, and then cooled to ambient temperature. Subsequently, the

temperature was increased to 300 °C at 10 °C min$^{-1}$, and the corresponding components of NO/N$_2$, C$_3$H$_6$/N$_2$, and O$_2$ were purged as needed, and the IR spectrum was recorded continuously.

### 2.3 Catalytic performance evaluation

The catalyst was sieved to 40–60 mesh and packed in quartz tubes (4 mm i.d.). The model flus gas was composed of 0.05 vol% NO, 0.3 vol% C$_3$H$_6$, 5 vol% O$_2$, and balanced with N$_2$. The NO$_x$ and C$_3$H$_6$ conversion were calculated in terms of the eqn (1) and (2), respectively, and the CO$_x$ selectivity was calculated in terms of the eqn (3):

$$\text{De-NO}_x \text{ efficiency} = \frac{[NO_x]_{in} - [NO_x]_{out}}{[NO_x]_{in}} \times 100\% \quad (1)$$

$$\text{C}_3\text{H}_6 \text{ conversion} = \frac{[C_3H_6]_{in} - [C_3H_6]_{out}}{[C_3H_6]_{in}} \times 100\% \quad (2)$$

$$\text{CO}_x \text{ selectivity} = \frac{[CO_x]}{3 \times ([C_3H_6]_{in} - [C_3H_6]_{out})} \times 100\% \quad (3)$$

where the subscript 'in' and 'out' represents volume concentration at the steady state. The total flow rate of 240 mL min$^{-1}$, and the corresponding weight hourly space velocity (WHSV) was 36 000 mL g$^{-1}$ h$^{-1}$. NO$_x$ concentrations were measured with an online NO$_x$ analyzer (Thermo Fisher, 42i-LH), and C$_3$H$_6$, CO and CO$_2$ concentrations were measured by gas chromatography (Fuli, GC 9790II).

## 3. Results and discussion

### 3.1 Texture properties

XRD patterns for 1Sn/γ-Al$_2$O$_3$, 5Ag/γ-Al$_2$O$_3$, 1Sn5Ag/γ-Al$_2$O$_3$ catalysts are presented in Fig. 1, where diffraction peaks observed for all the catalysts at $2\theta$ = 19.6°, 32.2°, 37.5°, 39.6°, 46.0°, 60.1°, and 66.7° were ascribed to γ-Al$_2$O$_3$ (JCPDS #02-1420), indexed to (111), (220), (311), (222), (400), (511), and (440) crystal planes, respectively. This also suggests that the loading of Ag and Sn active components did not disrupt the crystalline structure of the support. In addition, no diffraction peaks belonging to the corresponding metals or oxides of Ag and Sn were detected on any of the catalysts, indicating that Ag and Sn species remained in the amorphous state on the γ-Al$_2$O$_3$ support. It was noted that the 1Sn5Ag/γ-Al$_2$O$_3$ catalyst showed significantly different diffraction peaks at $2\theta$ = 27.6°, 32.1°, 46.2°, 54.8°, 57.5°, and 76.8° from the other two catalysts, which were all ascribed to the diffraction peaks of AgCl crystalline. This should be related to the fact that the precursor of tin used for catalyst preparation was SnCl$_4$ as mentioned in Section 2.1. The specific surface area loss for 1Sn5Ag/γ-Al$_2$O$_3$ catalyst might be related to the formation of AgCl crystallites as well.

N$_2$ adsorption–desorption was carried out to obtain the specific surface area and pore structure of the catalysts, the results of which are shown in Table 1 and Fig. 2. It can be seen that the loading of Sn or Ag had little effect on the specific surface area, and the values of 1Sn/γ-Al$_2$O$_3$ and 5Ag/γ-Al$_2$O$_3$
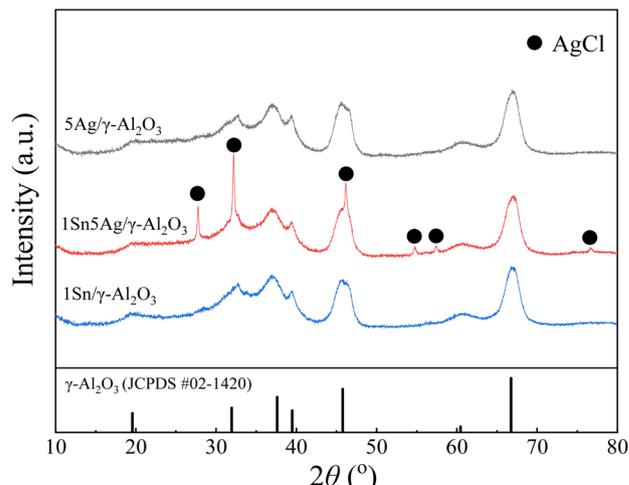


**Fig. 1** XRD patterns of 1Sn/γ-Al$_2$O$_3$, 5Ag/γ-Al$_2$O$_3$, and 1Sn5Ag/γ-Al$_2$O$_3$ catalysts.

were very close to the γ-Al$_2$O$_3$ support (180.10 m$^2$ g$^{-1}$). However, the catalysts loaded with both Sn and Ag (1Sn5Ag/γ-Al$_2$O$_3$) were found to show an obvious surface area loss, and it exhibited the lowest specific surface area (172.2 m$^2$ g$^{-1}$). This is possibly due to the precipitation of Ag and Sn species into the channel of γ-Al$_2$O$_3$, resulting in a reduction in the specific surface area of the catalysts.[30] The change in pore volume and pore size of the catalysts showed a slight decrease in pore volume and pore size after loading. As shown in Fig. 2a, the adsorption–desorption isotherms of the 1Sn/γ-Al$_2$O$_3$, 5Ag/γ-Al$_2$O$_3$, and 1Sn5Ag/γ-Al$_2$O$_3$ catalysts were all of type IV, and the hysteresis loops were of type H2b. This suggests the mesoporous structure of the catalysts, and the loading of Sn and Ag had little effect on the pore structure. The pore size distributions of the three catalysts were also similar, with the pore sizes mainly in the mesoporous range of 2–30 nm (Fig. 2b).

Fig. 3 demonstrates the micrographs of 1Sn/γ-Al$_2$O$_3$, 5Ag/γ-Al$_2$O$_3$, and 1Sn5Ag/γ-Al$_2$O$_3$, and energy dispersive spectrometer (EDS) mapping of 1Sn5Ag/γ-Al$_2$O$_3$. Small particles belonging to Sn and Ag species were observed, and the particle sizes mainly fell into the range of 20–50 nm (Fig. 3a–f). EDS mapping of 1Sn5Ag/γ-Al$_2$O$_3$ detected a uniform distribution of Ag, Sn, and Cl elements on the catalyst surface (Fig. 3g–i), indicating a high

**Table 1** The specific surface area, pore volume, and pore size of γ-Al$_2$O$_3$, 1Sn/γ-Al$_2$O$_3$, 5Ag/γ-Al$_2$O$_3$, and 1Sn5Ag/γ-Al$_2$O$_3$ catalysts

| Catalysts | $S_{BET}$ (m$^2$ g$^{-1}$) | Pore volume$^a$ (cm$^3$ g$^{-1}$) | Pore size$^b$ (nm) |
|---|---|---|---|
| γ-Al$_2$O$_3$ | 180.1 | 0.68 | 10.2 |
| 1Sn/γ-Al$_2$O$_3$ | 186.2 | 0.58 | 8.3 |
| 5Ag/γ-Al$_2$O$_3$ | 177.8 | 0.55 | 9.9 |
| 1Sn5Ag/γ-Al$_2$O$_3$ | 172.2 | 0.54 | 9.5 |

$^a$ BJH desorption cumulative volume of pores. $^b$ BJH desorption average pore diameter.

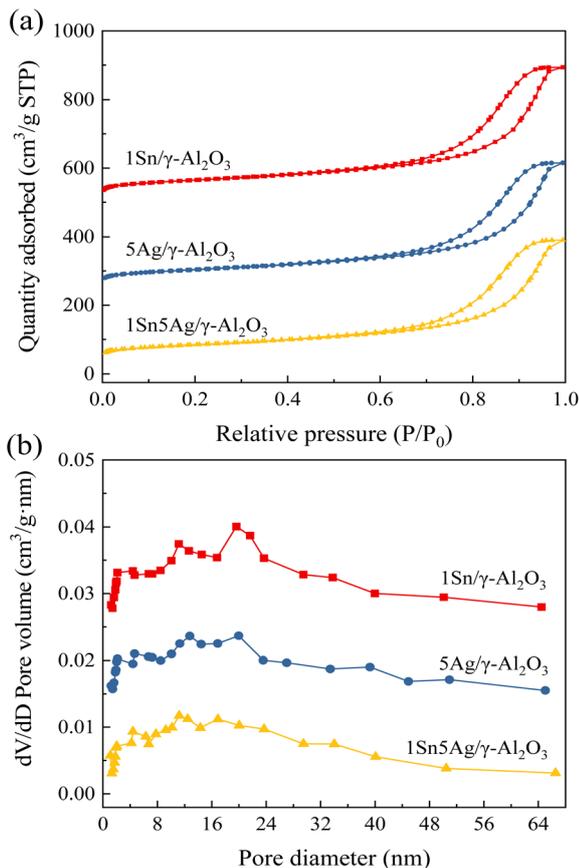**Fig. 2** $N_2$ adsorption–desorption isotherms (a) and pore diameter distribution (b) of $\gamma$-$Al_2O_3$, $1Sn/\gamma$-$Al_2O_3$, $5Ag/\gamma$-$Al_2O_3$, and $1Sn5Ag/\gamma$-$Al_2O_3$ catalysts.

dispersion of Ag and Sn species on the surface of $1Sn5Ag/\gamma$-$Al_2O_3$ catalyst. Besides, it was noted that the $1Sn5Ag/\gamma$-$Al_2O_3$ had rod-like components with larger size that were distinct from $1Sn/\gamma$-$Al_2O_3$ and $5Ag/\gamma$-$Al_2O_3$. In combination with the XRD results, it was speculated that these rod-like components were probably AgCl species. Furthermore, the states of Ag and Sn species of the $1Sn5Ag/\gamma$-$Al_2O_3$ catalyst were determined by HR-TEM, and the representative micrographs are shown in Fig. 3j–l. Both $\gamma$-$Al_2O_3$ support exposing the (111) crystal plane and AgCl crystallites exposing the (220) crystal plane could be clearly observed, which corresponded well to the XRD patterns presented in Fig. 1. Besides, many areas with instinct lattice fringe were also found. This implies that a mass of amorphous phases also existed in the catalyst. Combined with the catalyst preparation and XRD results, it was deduced that the amorphous phases were highly dispersed oxides of Sn and Ag. To sum up, the pore structure and morphological characteristics of the catalysts were little affected by Sn and Ag loading, indicating that the increased de-$NO_x$ activity of $1Sn5Ag/\gamma$-$Al_2O_3$ might be mainly due to changes in its chemical properties.

### 3.2 Chemical states of surface elements

High-resolution XPS was performed to determine the chemical states of the elements on the surface of catalysts. The spectra of

O 1s, Sn 3d, and Ag 3d of $1Sn/\gamma$-$Al_2O_3$, $5Ag/\gamma$-$Al_2O_3$, and $1Sn5Ag/\gamma$-$Al_2O_3$ catalysts, and their deconvolution results are presented in Fig. 4. The Sn 3d spectrum on $1Sn/\gamma$-$Al_2O_3$ catalyst (Fig. 4a), where the binding energies at 495.35 and 495.35 eV are $3d_{5/2}$ and $3d_{3/2}$ resulting from Sn 3d spin–orbit coupling, respectively. This indicates that the Sn species mainly exists in the form of $Sn^{4+}$,[24] which were active sites in $C_3H_6$-SCR reaction.[31] However, when Ag and Sn were co-loaded, the binding energies of Sn $3d_{3/2}$ and Sn $3d_{5/2}$ of $1Sn5Ag/\gamma$-$Al_2O_3$ shifted from 495.35 eV to 495.5 eV and 486.65 eV to 486.8 eV, respectively. This indicated that the Sn 3d electron cloud density of $1Sn5Ag/\gamma$-$Al_2O_3$ catalyst decreased, which was possibly due to the electron transfer from Sn to Ag species, and the strong electronegativity of $Cl^-$ might contribute as well.

Two XPS characteristic peaks of Ag 3d, $3d_{5/2}$ and $3d_{3/2}$, were observed, and they could be deconvoluted into $Ag^+$ and $Ag^0$ (ref. 29) (Fig. 4b). The ratio of $Ag^0/Ag^+$ was calculated to be 2.15 for $5Ag/\gamma$-$Al_2O_3$ and 3.68 for $1Sn5Ag/\gamma$-$Al_2O_3$, respectively. The coexistence of Ag and Sn species on the surface of the $1Sn5Ag/\gamma$-$Al_2O_3$ resulted in a significant increase in the relative $Ag^0$ content, which was deduced to be the electron cloud transfer from Sn to Ag species. The existence of $Ag^0$ on the surface of $5Ag/\gamma$-$Al_2O_3$ catalyst was resulted from the strong metal-support interaction (SMSI) effects. In combination with the XRD results, it was concluded that the presence of Ag on the surface of the $5Ag/Al_2O_3$ was in the amorphous states of metallic $Ag^0$ and $Ag_2O$. The presence of Ag on the surface of the $1Sn5Ag/\gamma$-$Al_2O_3$ was in the amorphous states of metallic $Ag^0$, $Ag_2O$ and AgCl crystalline. The highly dispersed state of $Ag^0$ species had a positive effect on the SCR activity. Xu *et al.* found that metallic silver species were conducive to the partial oxidation of hydrocarbons and form active enolic species, thus the low-temperature catalytic efficiency was improved.[32] More *et al.*[9] also reported similar positive effects of $Ag^0$ species for $NO_x$ removal.

O 1s was deconvoluted into three peaks at 530.9, 533.1, and 532.2 eV, corresponding to surface lattice oxygen (denoted as $O_\beta$), surface adsorbed oxygen (denoted as $O_\alpha$), and surface hydroxyl (denoted as $O_\gamma$), respectively.[33] It is found that the relative ratios of $O_\alpha$ (0.33) and $O_\gamma$ (0.15) for $1Sn5Ag/\gamma$-$Al_2O_3$ were greatly increased compared to that of $1Sn/\gamma$-$Al_2O_3$ and $5Ag/\gamma$-$Al_2O_3$. It is well known that $O_\alpha$ species with high mobility are more favorable for the SCR process.[34] Besides, the $O_\gamma$ species were also important active sites for the adsorption and activation of $C_3H_6$ and NO, especially in the low temperature range.[13] The increased relative ratios of $O_\alpha$ and $O_\gamma$ species on the surface of $1Sn5Ag/\gamma$-$Al_2O_3$ made great contributions to its de-$NO_x$ activity improvement.

### 3.3 The mobility of surface oxygen species

The mobility of surface oxygen species on the surface of $1Sn/\gamma$-$Al_2O_3$, $5Ag/\gamma$-$Al_2O_3$ and $1Sn5Ag/\gamma$-$Al_2O_3$ catalysts were further studied by $H_2$-TPR and $O_2$-TPD, and the results are shown in Fig. 5. Due to the high temperature pretreatment of the $Al_2O_3$ support and its strong Al–O bond, no significant reduction peaks should be observed in the temperature range tested. As
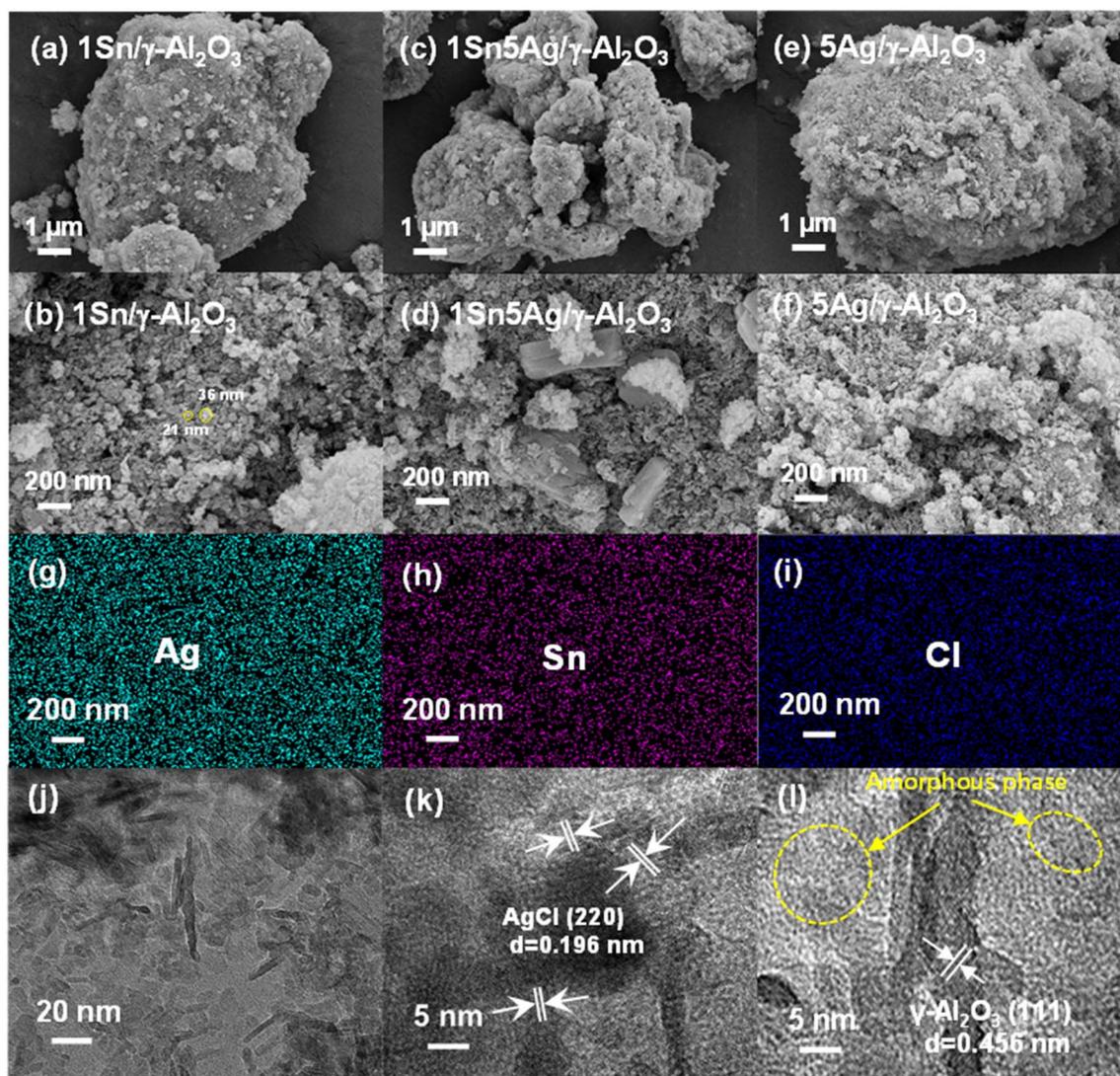
**Fig. 3** SEM images of 1Sn/γ-Al$_2$O$_3$ (a and b), 1Sn5Ag/γ-Al$_2$O$_3$ (c and d), and 5Ag/γ-Al$_2$O$_3$ (e and f) catalysts, EDS mapping of 1Sn5Ag/γ-Al$_2$O$_3$ catalyst (g–i), and TEM graphs of 1Sn5Ag/γ-Al$_2$O$_3$ catalyst (j–l).

presented in Fig. 5a, 1Sn/γ-Al$_2$O$_3$ showed only one H$_2$ reduction peak at 200 °C, which could be ascribed to Sn$^{4+}$ to Sn$^{2+}$ reduction peak. Two reduction peaks were observed at 91 °C and 123 °C for 5Ag/γ-Al$_2$O$_3$, probably corresponding to the Ag$^+$ reduction of AgCl and Ag$^+$ reduction of Ag$_2$O, respectively. In contrast, a broad reduction peak at 187 °C was observed for the 1Sn5Ag/γ-Al$_2$O$_3$, as well as a reduction peak at 533 °C. The peak at 187 °C should be an overlap of the Sn$^{4+}$ reduction peak and the Ag$^+$ reduction peak, while the peak at 533 °C was ascribed to the Sn$^{2+}$ to Sn$^0$ reduction peak.[23] Compared with 5Aag/γ-Al$_2$O$_3$, there was a significant increase in the number of reducible species for 1Sn5Ag/γ-Al$_2$O$_3$, but the reducibility was weakened. This indicates that a higher number of surface oxygen species on 1Sn5Ag/γ-Al$_2$O$_3$ could participate in the SCR reaction, but with a weaker mobility.

As shown in Fig. 5b, several O$_2$ desorption bands were clearly observed for the catalysts tested. It is generally considered that the desorption bands between 50 and 300 °C corresponded to surface adsorption oxygen species, and the bands between 300 and 600 °C corresponded to surface lattice oxygen species.[35] There was a broad band centered at 396 °C of 1Sn/γ-Al$_2$O$_3$, with the highest desorption temperature among the three catalysts, and this suggests that the surface oxygen species mobility of 1Sn/γ-Al$_2$O$_3$ was inferior to that of 5Ag/γ-Al$_2$O$_3$ and 1Sn5Ag/γ-Al$_2$O$_3$. By contrast, there was a broad desorption band centered at 209 °C of 5Ag/γ-Al$_2$O$_3$, indicating the high mobility of its surface adsorbed oxygen species. This also explains why it has the strongest ability to deeply oxidize C$_3$H$_6$ into CO$_2$. Besides, no desorption peaks attributed to lattice oxygen were detected for 5Ag/γ-Al$_2$O$_3$, indicating the inferior mobility of surface lattice oxygen species and they were difficult to participate in the SCR reaction. In comparison to the 5Ag/γ-Al$_2$O$_3$, the amount of adsorbed oxygen species on the surface of 1Sn5Ag/γ-Al$_2$O$_3$ increased, and the amount of total oxygen species desorbed was
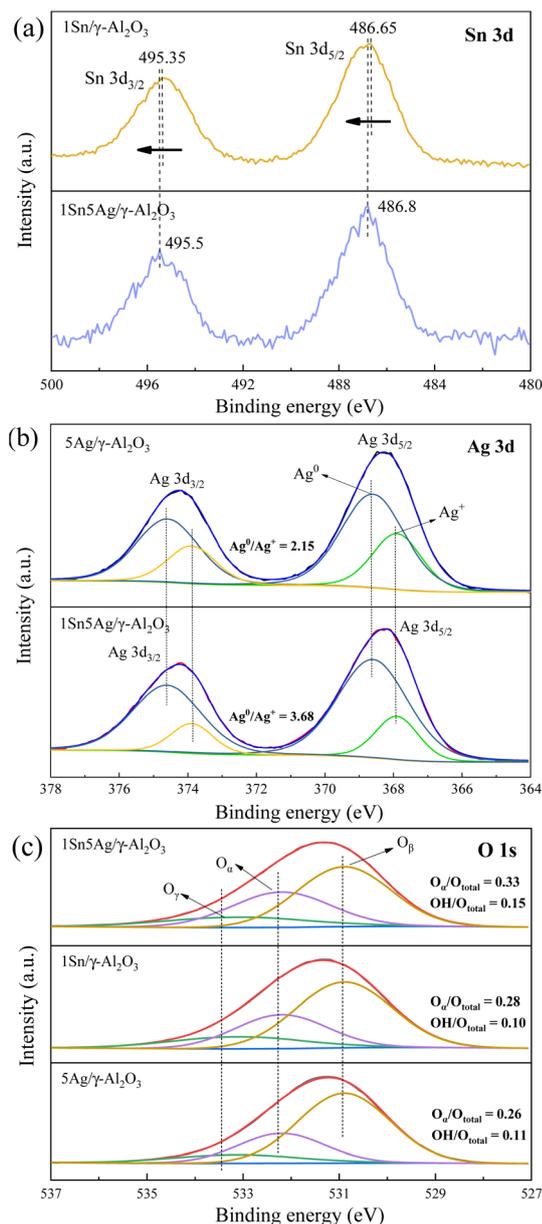
Fig. 4 XPS spectra of Sn 3d (a), Ag 3d (b), and O 1s (c) of 1Sn/γ-Al₂O₃, 5Ag/γ-Al₂O₃, and 1Sn5Ag/γ-Al₂O₃ catalysts.



Fig. 5 H₂-TPR (a) and O₂-TPD (b) profiles of 1Sn/γ-Al₂O₃, 5Ag/γ-Al₂O₃, and 1Sn5Ag/γ-Al₂O₃ catalysts.

over-oxidation of $C_3H_6$ to $CO_2$, thus the de-$NO_x$ efficiency was improved.

### 3.4 Surface acidity properties

Py-IR was carried out to identify the nature of surface acid sites, which is another determining factor for $C_3H_6$-SCR performance, and the results of 1Sn5Ag/γ-Al₂O₃ catalyst are shown in Fig. 6. The bands at 1450 and 1575 cm⁻¹ were assigned to the pyridine molecule (Py-L)[37] adsorbed on the Lewis acid sites, and the band at 1612 cm⁻¹ was assigned to Lewis–Brønsted acid complex,[18,37] the band at 1612 cm⁻¹ was assigned to the adsorbed pyridine ion (Py-H⁺).[38] It is worth noting that compared with the number of Lewis acid sites, Brønsted acid sites were extremely lacking. There were only a few Brønsted acid sites on the surface of the 5Ag/γ-Al₂O₃ catalyst, and none for 1Sn5Ag/γ-Al₂O₃. Some researchers reported that the Brønsted acid sites were indispensable for $C_3H_6$-SCR reaction, because they played a key role in $C_3H_6$ activation and forming related intermediates.[36,39] However, Lewis acids were found to be essential for NO adsorption, which was a key step in $C_3H_6$-SCR,[40] and the adsorption strength was stronger than on Brønsted acid sites.[41] Hence, it was deduced that for the 1Sn5Ag/γ-Al₂O₃ catalyst, the adsorption and activation of $C_3H_6$ and NO were mainly achieved at the Lewis acid sites, i.e., the Lewis acids dominated $C_3H_6$-SCR

the largest. Besides, it is noted that the surface adsorbed oxygen desorption temperature of 1Sn5Ag/γ-Al₂O₃ shifted to 190 °C and became weaker, but a new surface lattice oxygen desorption band (296 °C) appeared. The decrease in the number of adsorbed oxygen species on the surface of 1Sn5Ag/γ-Al₂O₃ inhibited the over-oxidation of $C_3H_6$, while the high mobility of surface lattice oxygen was conducive to partial oxidation of $C_3H_6$.[36] Therefore, 1Sn5Ag/γ-Al₂O₃ catalyst showed better de-$NO_x$ efficiency. The combined results of O₂-TPD and H₂-TPR showed that the redox ability of the catalyst was effectively regulated by co-loading Sn and Ag. The coexistence of Sn and Ag promoted the oxidation of $C_3H_6$ and NO to acetates, nitrates and other important intermediates on 1Sn5Ag/γ-Al₂O₃, but inhibited the

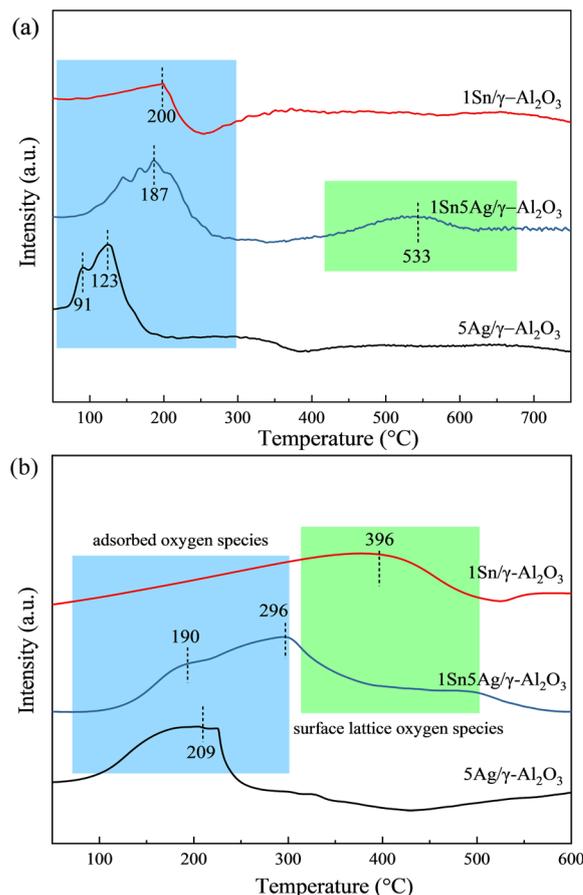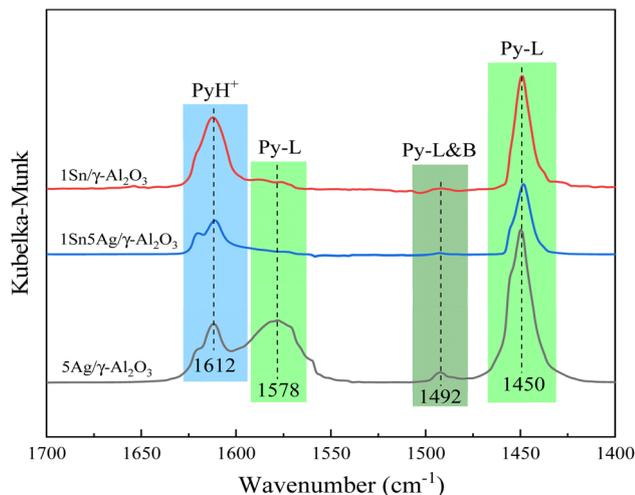Fig. 6 DRIFTS of pyridine adsorption on $5Ag/\gamma$-$Al_2O_3$, $1Sn/\gamma$-$Al_2O_3$, and $1Sn5Ag/\gamma$-$Al_2O_3$ catalysts at 300 °C.

reaction. Besides, Lin *et al.*[42] reported that Lewis acid sites were responsible for deep oxidation of $C_3H_6$. The $5Ag/\gamma$-$Al_2O_3$ catalyst had the largest number of Lewis acid sites, which explains why it exhibited the highest $C_3H_6$ conversion. In comparison, total acid content and acid strength of $1Sn5Ag/\gamma$-$Al_2O_3$ greatly decreased, thus inhibited $C_3H_6$ over-oxidation into $CO_2$, which was beneficial to the improvement of the de-$NO_x$ efficiency. A similar phenomenon was also observed for $C_3H_6$-SCR over Mg–Ag/$Al_2O_3$ catalyst.[10] The above studies revealed that the improved de-$NO_x$ efficiency for $1Sn5Ag/\gamma$-$Al_2O_3$ catalyst was largely attributed to the synergistic effect between Sn and Ag species, which positively changed their chemical states, the mobility of surface oxygen species and surface acidity for $C_3H_6$-SCR.

### 3.5 Catalytic activity

Ag species with various amounts were loaded onto $1Sn/\gamma$-$Al_2O_3$, and the results are shown in Fig. 7a. It is seen that the de-$NO_x$ efficiency was somewhat suppressed after the introduction of 1 wt% Ag component onto $1Sn/\gamma$-$Al_2O_3$. As the Ag loading was increased 5 wt%, the overall de-$NO_x$ efficiency reached the highest level. The $1Sn5Ag/\gamma$-$Al_2O_3$ catalyst showed the widest temperature window of $T_{80}$ (the temperature at which 80% de-$NO_x$ efficiency was achieved), which was 336–448 °C, and it reached a maximum de-$NO_x$ efficiency of 88% at 400 °C. At 350 °C, the $1Sn5Ag/\gamma$-$Al_2O_3$ catalyst achieved *ca.* 50% higher de-$NO_x$ activity than $1Sn/\gamma$-$Al_2O_3$, and *ca.* 15% higher than $5Ag/\gamma$-$Al_2O_3$. Several representative metal oxides supported catalysts were compiled in Table 2 and the de-$NO_x$ efficiency at 350 °C was compared with $1Sn5Ag/\gamma$-$Al_2O_3$ catalyst. However, a further increase of Ag loading to 10 wt% resulted in a significant decrease in de-$NO_x$ efficiency. This might be attributed to the high Ag loading resulting in a large amount of $C_3H_6$ being over-oxidized into $CO_2$ and thus less involved in $NO_x$ reduction. Based on the above results, there were obvious synergistic effects between the Sn and Ag components supported on $\gamma$-
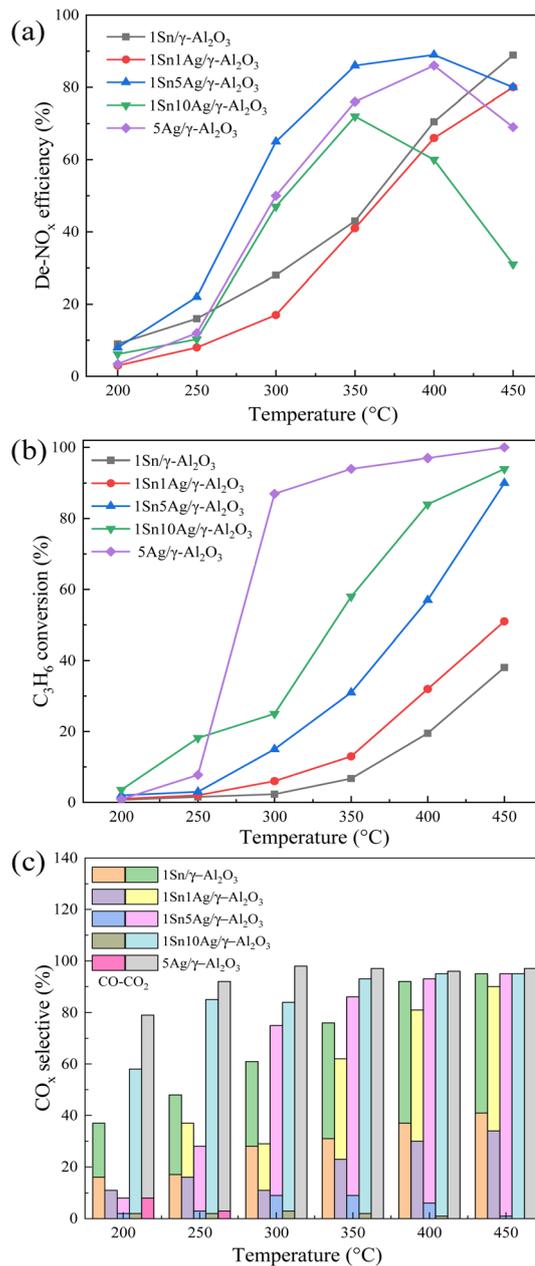


Fig. 7 The de-$NO_x$ efficiency (a), $C_3H_6$ conversion (b), and $CO_x$ selectivity (c) over $1Sn/\gamma$-$Al_2O_3$, $5Ag/\gamma$-$Al_2O_3$, $1Sn1Ag/\gamma$-$Al_2O_3$, $1Sn5Ag/\gamma$-$Al_2O_3$, and $1Sn10Ag/\gamma$-$Al_2O_3$ catalysts. Reaction conditions: 0.05% NO, 0.3% $C_3H_6$, 5% $O_2$, and $N_2$ balance.

$Al_2O_3$, and the best de-$NO_x$ efficiency was achieved when the loading amount of Sn and Ag was 1 wt% and 5 wt%, respectively.

Fig. 7b and c demonstrate the $C_3H_6$ conversion and $CO_x$ selectivity. It is seen that the $5Ag/\gamma$-$Al_2O_3$ catalyst achieved the highest conversion for the catalytic oxidation of $C_3H_6$, and the $CO_2$ selectivity was close to 100% at 300 °C. However, the deep oxidation of $C_3H_6$ was unfavorable for its participation in the SCR process. In the $C_3H_6$-SCR process, the reaction of $C_3H_6$ with $NO_x$ and the direct oxidation of $C_3H_6$ are in competition, and the $NO_x$ reduction mainly depends on the intermediate species

**Table 2** De-NO$_x$ efficiency of representative metal oxides supported catalysts

| Catalysts | Reaction conditions/vol% | WHSV/mL g$^{-1}$ h$^{-1}$ | $T_{80}$/°C | De-NO$_x$ efficiency at 350 °C/% | Ref. |
|---|---|---|---|---|---|
| SnO$_2$/Beta | 0.05% NO, 0.05% C$_3$H$_6$, 5% O$_2$ | 60 000 | 470 | 13 | 24 |
| SnO$_2$/ZSM-5 | 0.05% NO, 0.05% C$_3$H$_6$, 5% O$_2$ | 60 000 | 446 | 35 | 11 |
| SnO$_2$/Al$_2$O$_3$ | 0.05% NO, 0.05% C$_3$H$_6$, 5% O$_2$ | 60 000 | 448 | 32 | 23 |
| 5%Ag/Al$_2$O$_3$ | 0.08% NO, 0.1714% C$_3$H$_6$, 10% O$_2$, 10% H$_2$O | 20,0000 | 425 | 23 | 26 |
| 1.6%Au/Al$_2$O$_3$ | 0.21% H$_2$, 0.0385% NO, 0.04% C$_3$H$_6$, 8% O$_2$ | 40 000 | — | 40 | 44 |
| 2%Ag–CeZr | 0.2% NO, 0.2% C$_3$H$_6$, 10% O$_2$, 10% H$_2$ | 45 000 | 300 | 83 | 45 |
| Cu$_{0.71}$Fe$_{0.29}$-600c | 0.05% NO, 0.1% C$_3$H$_6$, 2% O$_2$ | 30 000 | — | 60 | 18 |
| Cu/SO$_4^{2-}$/Al–Ce-PILC | 0.22% NO, 0.12% C$_3$H$_6$, 2% O$_2$ | 30 000 | — | 47 | 42 |
| This work | 0.05% NO, 0.3% C$_3$H$_6$, 5% O$_2$ | 36 000 | 336 | 85 | — |
| | | 60 000 | — | 77 | |

such as acetates generated by the partial oxidation of C$_3$H$_6$.[43] Higher ratio of C$_3$H$_6$ being deeply oxidized to CO$_2$ resulted in less C$_3$H$_6$ for NO$_x$ reduction and thus deteriorated the de-NO$_x$ efficiency. It is seen that the C$_3$H$_6$ conversion of 1Sn5Ag/γ-Al$_2$O$_3$ catalyst at 300 °C was reduced by *ca.* 70% compared to that of 5Ag/γ-Al$_2$O$_3$ (Fig. 7b). The total CO$_x$ selectivity was *ca.* 75%, indicating that a large number of organic intermediates might have been generated on the surface of 1Sn5Ag/γ-Al$_2$O$_3$ catalyst. For the 1Sn1Ag/γ-Al$_2$O$_3$ catalyst, the CO$_x$ selectivity was the lowest overall among all samples tested (Fig. 7c), although its C$_3$H$_6$ conversion was slightly higher than that of 1Sn/γ-Al$_2$O$_3$. Moreover, the de-NO$_x$ efficiency was also lower than that of 1Sn/γ-Al$_2$O$_3$. This suggests that the oxidation of C$_3$H$_6$ possibly generated a certain number of intermediates over 1Sn1Ag/γ-Al$_2$O$_3$, and they exhibited inferior reactivity with NO$_x$. As for 1Sn10Ag/γ-Al$_2$O$_3$ catalyst, the decrease in de-NO$_x$ efficiency might be due to the higher amount of C$_3$H$_6$ over-oxidation after the Ag loading increases. The above results suggest that the synergistic effects between a certain proportion of Ag and Sn components maintained the oxidation of C$_3$H$_6$ at a suitable level, so that more reactive organic intermediates would be generated to participate in the SCR reaction, thus effectively improving the de-NO$_x$ efficiency.

### 3.6 Reaction mechanism

Firstly, the adsorption characteristics of C$_3$H$_6$ and NO molecules on the 1Sn5Ag/γ-Al$_2$O$_3$ catalyst were studied, and the corresponding FTIR bands at 30 °C are presented in Fig. 8. When C$_3$H$_6$ and O$_2$ were introduced, five bands emerged between 1200 and 1800 cm$^{-1}$. The band observed at 1383 cm$^{-1}$ was assigned to formate species.[15] The band at 1406 cm$^{-1}$ was assigned to enolic species.[29] The bands at 1456 and 1593 cm$^{-1}$ were assigned to acetate species.[46] The band at 1654 cm$^{-1}$ was assigned to the δ(OH) hydroxyl group of surface adsorbed water.[47] Besides, the broad band between 3000 and 3200 cm$^{-1}$ was ascribed to ν(C–H) of C$_3$H$_6$, and 3200–3500 cm$^{-1}$ was ascribed to hydrogen-bonded OH groups.[36] The above results indicate that C$_3$H$_6$ could be easily oxidized over 1Sn5Ag/γ-Al$_2$O$_3$ catalyst, and acetates were the main intermediates.

When NO and O$_2$ were introduced, four bands were observed between 1200 and 1800 cm$^{-1}$. The band at 1244 cm$^{-1}$ was

assigned to bridged nitrates. The bands at 1298 and 1554 cm$^{-1}$ were assigned to bidentate nitrates.[16] The bands at 1654 cm$^{-1}$ and 3200–3500 cm$^{-1}$ were assigned to surface hydroxyl groups. This indicates that NO could be easily oxidized over 1Sn5Ag/γ-Al$_2$O$_3$ catalyst to generate bridged nitrate and bidentate nitrate. In addition, it was noted that the surface hydroxyl groups (originated from the synergistic effects between Sn and Ag based on the XPS results) were largely consumed after the introduction of NO. Therefore, the presence of surface hydroxyl groups helped to promote the formation of key intermediate nitrates, and then effectively improve the low-temperature de-NO$_x$ activity.

The transient reaction experiments were carried out to further explore the C$_3$H$_6$-SCR mechanism of 1Sn5Ag/γ-Al$_2$O$_3$ catalyst. At first, C$_3$H$_6$ and O$_2$ were pre-adsorbed on the surface of 1Sn5Ag/γ-Al$_2$O$_3$ catalyst at 300 °C, and then NO was introduced. The results of the bands changes at different time durations are shown in Fig. 9a. The bands at 1296, 1456,
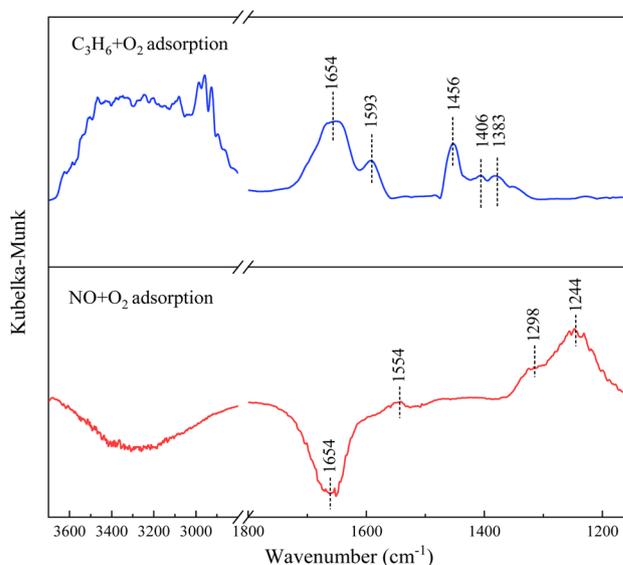


**Fig. 8** C$_3$H$_6$ + O$_2$ adsorption at 30 °C and NO + O$_2$ adsorption at 30 °C over 1Sn5Ag/γ-Al$_2$O$_3$ catalyst. Reaction conditions: 0.05% NO, 0.3% C$_3$H$_6$, 5% O$_2$, and N$_2$ balance.
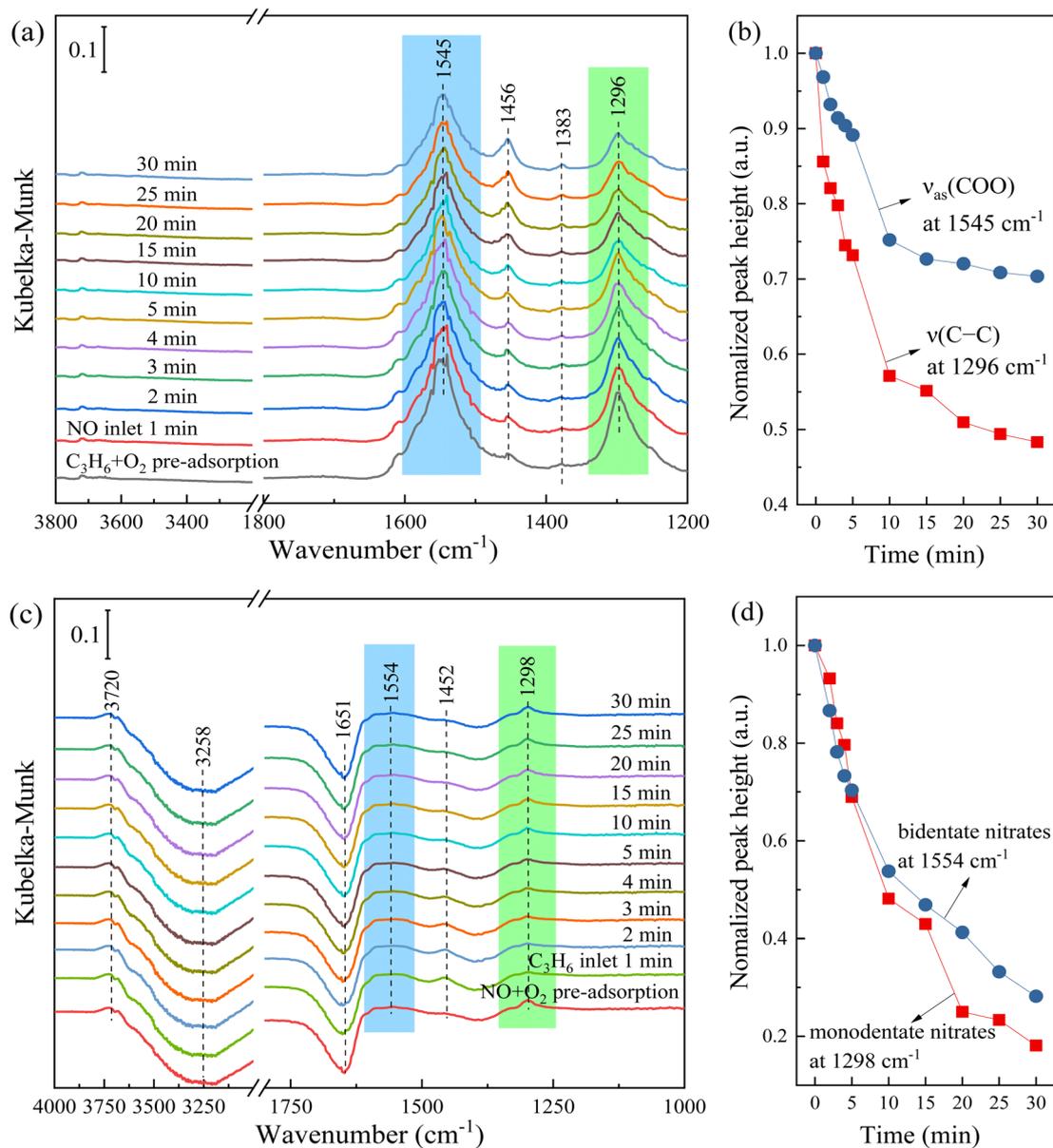
**Fig. 9** *In situ* DRIFTS of pre-adsorbed $C_3H_6$ and $O_2$ at 300 °C and followed by a flow of NO over 1Sn5Ag/$\gamma$-Al$_2$O$_3$ catalyst at different time durations (a), and normalized peak height changes of the band at 1545 and 1296 cm$^{-1}$ (b); *In situ* DRIFTS of pre-adsorbed NO and $O_2$ at 300 °C and followed by a flow of $C_3H_6$ at different time durations (c), and normalized peak height changes of the band at 1298 and 1554 cm$^{-1}$ (d). Reaction conditions: 0.05% NO, 0.3% $C_3H_6$, 5% $O_2$, and $N_2$ balance.

1545 cm$^{-1}$ were assigned to $\nu$(C–C), $\nu_s$(COO), and $\nu_{as}$(COO) of acetates.[26,27,48] Comparing with the FTIR spectra at 30 °C, it was found that the thermal stability of formates was quite high (1383 cm$^{-1}$), but the acetates would partially disappear (1456 and 1593 cm$^{-1}$) as the temperature was increased to 300 °C. Besides, it was noted that the bands at 1296 and 1545 cm$^{-1}$ were continuously consumed after NO was introduced, following the E-R mechanism. In contrast, formates were almost inert and did not react with NO. Fig. 9b show normalized peak height changes of the band at 1296 and 1545 cm$^{-1}$ with the time of NO feeding. It is seen that the acetates were quickly consumed within 10 min, indicating that acetates were key active

intermediates involved in the $C_3H_6$-SCR reaction over 1Sn5Ag/$\gamma$-Al$_2$O$_3$ catalyst. Acetates with high reactivity were also detected over Ag/Al$_2$O$_3$ and Cu/Al$_2$O$_3$ catalysts, and being consumed at a similar rate to NO$_x$.[49–51] The band at 1456 cm$^{-1}$ was possibly ascribed to the overlapping of acetates and monodentate nitrates, because monodentate nitrates would accumulate with the continuous flow of NO while acetates should be consumed.

Subsequently, NO and $O_2$ were pre-adsorbed on the surface of 1Sn5Ag/$\gamma$-Al$_2$O$_3$ catalyst at 300 °C, and then $C_3H_6$ was introduced. The results of the bands changes at different time durations are shown in Fig. 9c. The bands at 1298 and 1456 cm$^{-1}$ were assigned to monodentate nitrates, and the

band at 1554 cm$^{-1}$ was assigned to bidentate nitrates. Comparing with the FTIR spectra at 30 °C, it was found that the bridge nitrates was not thermally stable, and it could be converted into monodentate and bidentate nitrates at elevated temperature. It is also noted in the FTIR bands belonging to monodentate nitrate (1456 cm$^{-1}$) and bidentate nitric acid (1554 cm$^{-1}$) were gradually consumed as $C_3H_6$ was introduced, following the E–R mechanism. The negative band assigned to adsorbed water at 1654 cm$^{-1}$ was gradually weakened with the introduction of $C_3H_6$, which was related to the formation of the R–$NO_2$ intermediates (1651 cm$^{-1}$).[14] Fig. 9d demonstrate the consumption rates of monodentate nitrates and bidentate nitrates as $C_3H_6$ was introduced, and both were consumed *ca.* 80% within 30 min. Besides, no accumulation of acetates was observed. Combined with the results in Fig. 9a, it suggests that the reactivity between gaseous $C_3H_6$ and adsorbed nitrates was higher than that of gaseous NO and adsorbed acetates. This is also consistent with the Py-IR results that the Lewis acid sites dominate nitrate species formation and activation. Besides, it is speculated that the nitrate species adsorbed on the hydroxyl group on the surface of the catalyst also participates in the SCR reaction, because with the introduction of $C_3H_6$, the band at 3258 cm$^{-1}$ assigned to the surface hydroxyl group weakened gradually, and water (3720 cm$^{-1}$) was formed at the same time.

Besides, NO + $C_3H_6$ + $O_2$ was introduced simultaneously between 200 and 500 °C, and the results are shown in Fig. 10. A new band at 2325 cm$^{-1}$ emerged, and it was assigned to NCO species.[52] NCO was also a key active intermediate for Ag/$Al_2O_3$ catalysts,[52] which was formed through the reaction between acetates and nitrates, and was easily further oxidized into $CO_2$ and $N_2$. Xu *et al.*[46] and Guo *et al.*[12] also reported that NCO species played an important role in improving $C_3H_6$-SCR process. The band assigned to NCO did not appear under the pre-adsorption reaction conditions, indicating that the SCR reaction of the 1Sn5Ag/$\gamma$-$Al_2O_3$ catalyst not only followed the E-
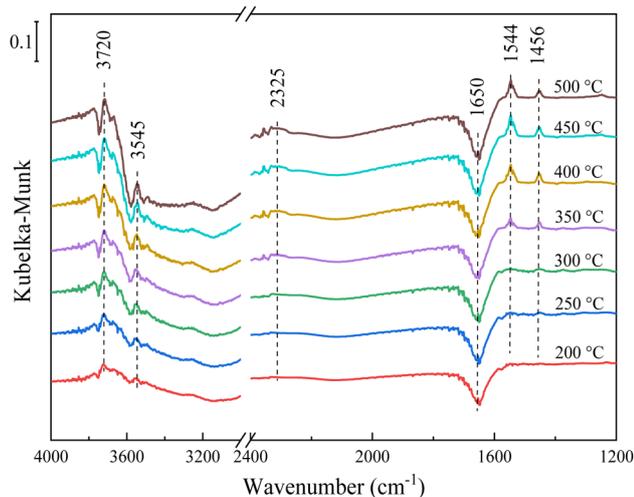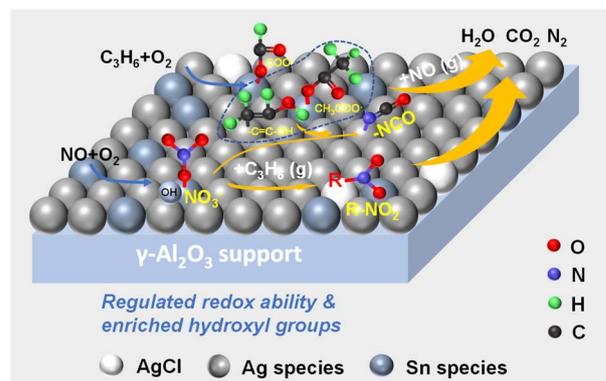


**Scheme 1** Proposed reaction mechanism of $C_3H_6$-SCR over 1Sn5Ag/$\gamma$-$Al_2O_3$ catalyst.

R mechanism, but also followed the L-H mechanism. Besides, the band assigned to NCO at 300 °C and below was very weak. With the increase of the reaction temperature, the amount of NCO generated increases, indicating that the formation of NCO was quite limited by the reaction kinetics at low temperature. The low amount NCO produced was responsible for the inferior de-$NO_x$ efficiency. With the further increase of the reaction temperature, the monodentate and bidentate nitrates accumulated and could not be further converted, thus deteriorated the de-$NO_x$ efficiency. The band assigned to water at 3545 and 3720 cm$^{-1}$ became stronger with the increase of temperature, which might be related to the SCR reaction and the direct oxidation of $C_3H_6$.

Based on the results of catalyst characterizations and *in situ* DRIFTS, the $C_3H_6$-SCR reaction mechanism over 1Sn5Ag/$\gamma$-$Al_2O_3$ catalyst was proposed and depicted in Scheme 1. The Lewis acid sites were mainly responsible for the $C_3H_6$-SCR reaction. A majority of $C_3H_6$ would therefore be partially oxidized into adsorbed formates, acetates and enolic species, and NO would be oxidized into monodentate and bidentate nitrates, on 1Sn5Ag/$\gamma$-$Al_2O_3$ catalyst. The presence of AgCl particles and hydroxyl species helped to promote the reactions. The reaction mainly occurred between adsorbed acetates and nitrates to form NCO species, and gaseous $C_3H_6$ with adsorbed monodentate and bidentate to form R–$NO_2$ species, and $CO_2$ and $N_2$ would be finally generated.

## 4. Conclusion

In this work, a series of Sn/$\gamma$-$Al_2O_3$ and SnAg/$\gamma$-$Al_2O_3$ catalysts with different loadings were prepared and tested, and it was found that the 1Sn5Ag/$\gamma$-$Al_2O_3$ catalyst exhibited the best $C_3H_6$-SCR activity, which maintained above 80% de-$NO_x$ efficiency between 336 and 448 °C. The synergistic effects of Sn and Ag improved the $C_3H_6$-SCR activity effectively. The characterizations found that the improvement of the de-$NO_x$ activity of 1Sn5Ag/$\gamma$-$Al_2O_3$ was closely related to the formation of AgCl nanoparticles, the change of Ag valence state, and the improvement of the mobility of surface oxygen species. The surface oxygen species contributed to the adsorption and



**Fig. 10** *In situ* DRIFTS spectra of 1Sn5Ag/$\gamma$-$Al_2O_3$ catalyst in a flow of NO + $C_3H_6$ + $O_2$ from 200 to 500 °C. Reaction conditions: 0.05% NO, 0.3% $C_3H_6$, 5% $O_2$, and $N_2$ balance.

activation of gaseous $C_3H_6$ and NO, and the highly dispersed metallic Ag species could promote the partial oxidation of $C_3H_6$ to enolic species with high reactivity. The presence of AgCl nanoparticles adjusted the redox ability of 1Sn5Ag/$\gamma$-$Al_2O_3$ to a moderate level and inhibited the deep oxidation of $C_3H_6$, which was essential for $C_3H_6$-SCR. The Lewis acid sites were mainly responsible for $C_3H_6$-SCR over 1Sn5Ag/$\gamma$-$Al_2O_3$ catalyst, and the reaction followed both E-R and L-H mechanism. The main reactions occurred between adsorbed monodentate/bidentate nitrates and gaseous $C_3H_6$, as well as acetates and nitrates, then key intermediates such as NCO and R–$NO_2$ would be generated. Finally, they would convert into harmless $N_2$ and $CO_2$. This work reveals the synergistic effects of noble and base metals (Ag and Sn) for promoting $C_3H_6$-SCR performance, which provided new theoretical ideas and guidance for developing new HC-SCR catalysts.

## Author contributions

Ning Li: investigation, writing – original draft, data curation; Tiantian Zhang: formal analysis; Zuliang Wu, Jing Li, Wei Wang, and Jiali Zhu: investigation; Shuiliang Yao: supervision; Erhao Gao: conceptualization, writing – review & editing, funding acquisition.

## Conflicts of interest

The authors declare that they have no known competing financial interests or personal relationships that could have appeared to influence the work reported in this paper.

## Acknowledgements

## References

1 X. Wang, X. Li, J. Mu, S. Fan, X. Chen, L. Wang, et al., Oxygen Vacancy-rich porous $Co_3O_4$ Nanosheets toward boosted NO reduction by CO and CO oxidation: insights into the structure-activity relationship and performance enhancement mechanism, ACS Appl. Mater. Interfaces, 2019, 11(45), 41988–41999.

2 H. Asakura, M. Kirihara, K. Fujita, S. Hosokawa, S. Kikkawa, K. Teramura, et al., Fe-modified CuNi Alloy catalyst as a nonprecious metal catalyst for three-way catalysis, Ind. Eng. Chem. Res., 2020, 59(45), 19907–19917.

3 T. Liu, J. Qian, Y. Yao, Z. Shi, L. Han, C. Liang, et al., Research on SCR of NO with CO over the $Cu_{0.1}La_{0.1}Ce_{0.8}O$ mixed-oxide catalysts: effect of the grinding, Mol. Catal., 2017, 430, 43–53.

4 Ministry of Ecology and Environment of the People's Republic of China, China mobile source environmental management annual report (Excerpt 2), Environ. Protect., 2021, 49(19), 60–70.

5 Y. Yu, X. Yi, J. Zhang, Z. Tong, C. Chen, M. Ma, et al., Application of $ReO_x$/$TiO_2$ catalysts with excellent $SO_2$ tolerance for the selective catalytic reduction of $NO_x$ by $NH_3$, Catal. Sci. Technol., 2021, 11(15), 5125–5134.

6 H. Zhou, Y. Su, W. Liao, W. Deng and F. Zhong, NO reduction by propane over monolithic cordierite-based Fe/$Al_2O_3$ catalyst: Reaction mechanism and effect of $H_2O$/$SO_2$, Fuel, 2016, 182, 352–360.

7 R. Raj, M. P. Harold and V. Balakotaiah, Kinetic modeling of NO selective reduction with $C_3H_6$ over Cu-SSZ13 monolithic catalyst, Chem. Eng. J., 2014, 254, 452–462.

8 G. Liu, D. Han, J. Cheng, Y. Feng, W. Quan, L. Yang, et al., Performance of $C_2H_4$ Reductant in activated-carbon-supported $MnO_x$-based SCR catalyst at low temperatures, Energies, 2019, 12, 123.

9 P. M. More, D. L. Nguyen, P. Granger, C. Dujardin, M. K. Dongare and S. B. Umbarkar, Activation by pretreatment of Ag-Au/$Al_2O_3$ bimetallic catalyst to improve low temperature HC-SCR of $NO_x$ for lean burn engine exhaust, Appl. Catal., B, 2015, 174, 145–156.

10 P. M. More, N. Jagtap, A. B. Kulal, M. K. Dongare and S. B. Umbarkar, Magnesia doped Ag/$Al_2O_3$-sulfur tolerant catalyst for low temperature HC-SCR of $NO_x$, Appl. Catal., B, 2014, 144, 408–415.

11 L. Zhang, Q. Lai, Y. Liu, X. Li, W. Zhang, X. Xu, et al., Study on the monolayer dispersion behavior of $SnO_2$ on ZSM-5 for $NO_x$-SCR by $C_3H_6$: the remarkable promotional effects of air plasma treatment, Phys. Chem. Chem. Phys., 2022, 24(7), 4212–4225.

12 J. Xu, T. Tang, Q. Zhang, C. Zhang and F. Guo, Remarkable low temperature catalytic activity for SCR of NO with propylene under oxygen-rich conditions over $Mn_{0.2}La_{0.07}Ce_{0.05}O_x$/ZSM-5 catalyst, Vacuum, 2021, 188, 110174.

13 J. Xu, T. Tang, X. Sheng, Y. Zhang, Q. Zhang and F. Guo, Excellent activity caused by dielectric barrier discharge (DBD) plasma activation for selective catalytic reduction with propylene ($C_3H_6$-SCR): Insight into the low temperature catalytic behavior of Mn/ZSM-5 catalysts, J. Environ. Chem. Eng., 2022, 10(2), 107009.

14 N. Wen, Y. Su, W. Deng, H. Zhou, M. Hu and B. Zhao, Synergy of CuNiFe-LDH based catalysts for enhancing low-temperature SCR-$C_3H_6$ performance: surface properties and reaction mechanism, Chem. Eng. J., 2022, 438, 135570.

15 Y. Su, N. Wen, J. Cheng, W. Deng, H. Zhou and B. Zhao, Experimental study on SCR-$C_3H_6$ over Cu-Fe/Al-PILC catalysts: catalytic performance, characterization, and mechanism, Ind. Eng. Chem. Res., 2020, 59(33), 14776–14788.

16 L. Ma, C. Y. Seo, X. Chen, K. Sun and J. W. Schwank, Indium-doped $Co_3O_4$ nanorods for catalytic oxidation of CO and $C_3H_6$ towards diesel exhaust, Appl. Catal., B, 2018, 222, 44–58.

17 M. Kashif, M. N. Khan, Y. Su and P. M. Heynderickx, Most efficient mesoporous Mn/Ga-PCH catalyst for low-temperature selective catalytic reduction of NO with $C_3H_6$, *Vacuum*, 2022, **198**, 110879.

18 N. Wen, Y. Su, W. Deng, H. Zhou and B. Zhao, Selective catalytic reduction of NO with $C_3H_6$ over CuFe-containing catalysts derived from layered double hydroxides, *Fuel*, 2021, **283**, 119296.

19 L. F. Liotta, G. Pantaleo, A. Macaluso, G. Di Carlo and G. Deganello, $CoO_x$ catalysts supported on alumina and alumina-baria: influence of the support on the cobalt species and their activity in NO reduction by $C_3H_6$ in lean conditions, *Appl. Catal., A*, 2003, **245**(1), 167–177.

20 T. Thiruppathiraja, A. L. Arokiyanathan and S. Lakshmipathi, Pyrrolic, pyridinic, and graphitic sumanene as metal-free catalyst for oxygen reduction reaction – A density functional theory study, *Fuel Cells*, 2021, **21**(6), 490–501.

21 N. Rajkoomar, A. Murugesan, S. Prabu and R. M. Gengan, Synthesis of methyl piperazinyl-quinolinyl alpha-aminophosphonates derivatives under microwave irradiation with Pd-SrTiO(3)catalyst and their antibacterial and antioxidant activities, *Phosphorus Sulfur Silicon Relat. Elem*, 2020, **195**(12), 1031–1038.

22 P. W. Park, H. H. Kung, D. W. Kim and M. C. Kung, Characterization of $SnO_2/Al_2O_3$ lean $NO_x$ catalysts, *J. Catal.*, 1999, **184**(2), 440–454.

23 Y. Liu, Q. Lai, Y. Sun, X. Xu, X. Fang, Y. Liu, *et al.*, $SnO_2/Al_2O_3$ catalysts for selective reduction of $NO_x$ by propylene: on the promotional effects of plasma treatment in air atmosphere, *Catal. Today*, 2019, **337**, 171–181.

24 Q. Lai, Y. Liu, L. Zhang, X. Li, Z. Qiu, X. Xu, *et al.*, Expounding the monolayer dispersion threshold effect of $SnO_2$/Beta catalysts on the selective catalytic reduction of $NO_x$ ($NO_x$-SCR) by $C_3H_6$, *Mol. Catal.*, 2021, **504**, 111464.

25 T. Chaieb, L. Delannoy, C. Louis and C. Thomas, On the origin of the optimum loading of Ag on $Al_2O_3$ in the $C_3H_6$-SCR of $NO_x$, *Appl. Catal., B*, 2013, **142**, 780–784.

26 J. Wang, H. He, Q. C. Feng, Y. B. Yu and K. Yoshida, Selective catalytic reduction of $NO_x$ with $C_3H_6$ over an Ag/$Al_2O_3$ catalyst with a small quantity of noble metal, *Catal. Today*, 2004, **93–5**, 783–789.

27 H. He, C. B. Zhang and Y. B. Yu, A comparative study of Ag/$Al_2O_3$ and Cu/$Al_2O_3$ catalysts for the selective catalytic reduction of NO by $C_3H_6$, *Catal. Today*, 2004, **90**, 191–197.

28 H. He, X. Zhang, Q. Wu, C. Zhang and Y. Yu, Review of Ag/$Al_2O_3$-Reductant system in the selective catalytic reduction of $NO_x$, *Catal. Surv. Asia*, 2008, **12**(1), 38–55.

29 Z. Wang, G. Xu, X. Liu, T. Wei, Y. Yu and H. He, Investigation of water and sulfur tolerance of precipitable silver compound Ag/$Al_2O_3$ catalysts in $H_2$-assisted $C_3H_6$-SCR of $NO_x$, *ACS Omega*, 2020, **5**(45), 29593–29600.

30 G. Xu, J. Ma, L. Wang, W. Xie, J. Liu, Y. Yu, *et al.*, Insight into the origin of sulfur tolerance of Ag/$Al_2O_3$ in the $H_2$-$C_3H_6$-SCR of $NO_x$, *Appl. Catal., B*, 2019, **244**, 909–918.

31 Z. Liu, J. Li and J. Hao, Selective catalytic reduction of $NO_x$ with propene over $SnO_2/Al_2O_3$ catalyst, *Chem. Eng. J.*, 2010, **165**(2), 420–425.

32 G. Xu, Y. Yu and H. He, Silver valence state determines the water tolerance of Ag/Al2O3 for the $H_2$-$C_3H_6$-SCR of $NO_x$, *J. Phys. Chem. C*, 2018, **122**(1), 670–680.

33 Z. Wen, B. Huang, Z. Shi, Z. Yang, M. Dai, W. Li, *et al.*, Mechanism of Zn salt-induced deactivation of a Cu/activated carbon catalyst for low-temperature denitration via CO-SCR, *RSC Adv.*, 2022, **12**(24), 14964–14975.

34 H. Hu, S. Cai, H. Li, L. Huang, L. Shi and D. Zhang, In Situ DRIFTs investigation of the low-temperature reaction mechanism over Mn-Doped $Co_3O_4$ for the Selective catalytic reduction of $NO_x$ with $NH_3$, *J. Phys. Chem. C*, 2015, **119**(40), 22924–22933.

35 Y. Zheng, Y. Yu, H. Zhou, W. Huang and Z. Pu, Combustion of lean methane over $Co_3O_4$ catalysts prepared with different cobalt precursors, *RSC Adv.*, 2020, **10**(8), 4490–4498.

36 M. Yuan, Y. Su, W. Deng and H. Zhou, Porous clay heterostructures (PCHs) modified with copper ferrite spinel as catalyst for SCR of NO with $C_3H_6$, *Chem. Eng. J.*, 2019, **375**, 122091.

37 J. Datka, A. M. Turek, J. M. Jehng and I. E. Wachs, Acidic properties of supported niobium oxide catalysts: an infrared spectroscopy investigation, *J. Catal.*, 1992, **135**, 186–199.

38 A. Sultana, M. Haneda, T. Fujitani and H. Hamada, Influence of $Al_2O_3$ support on the activity of Ag/$Al_2O_3$ catalysts for SCR of NO with decane, *Catal. Lett.*, 2007, **114**(1–2), 96–102.

39 M. Yuan, W. Deng, S. Dong, Q. Li, B. Zhao and Y. Su, Montmorillonite based porous clay heterostructures modified with Fe as catalysts for selective catalytic reduction of NO with propylene, *Chem. Eng. J.*, 2018, **353**, 839–848.

40 D. Yuan, X. Li, Q. Zhao, J. Zhao, S. Liu and M. Tade, Effect of surface lewis acidity on selective catalytic reduction of NO by $C_3H_6$ over calcined hydrotalcite, *Appl. Catal., A*, 2013, **451**, 176–183.

41 Y. Wang, Z. Lei, B. Chen, Q. Guo and N. Liu, Adsorption of NO and $N_2O$ on Fe-BEA and H-BEA zeolites, *Appl. Surf. Sci.*, 2010, **256**(12), 4042–4047.

42 Q. Lin, J. Hao, J. Li, Z. Ma and W. Lin, Copper-impregnated Al-Ce-pillared clay for selective catalytic reduction of NO by $C_3H_6$, *Catal. Today*, 2007, **126**(3–4), 351–358.

43 Y. Yu, X. Zhang and H. He, Evidence for the formation, isomerization and decomposition of organo-nitrite and -nitro species during the $NO_x$ reduction by $C_3H_6$ on Ag/$Al_2O_3$, *Appl. Catal., B*, 2007, **75**(3–4), 298–302.

44 T. Chaieb, L. Delannoy, S. Casale, C. Louis and C. Thomas, Evidence for an $H_2$ promoting effect in the selective catalytic reduction of $NO_x$ by propene on Au/$Al_2O_3$, *Chem. Commun.*, 2015, **51**(4), 796–799.

45 J. Duan, L. Zhao, S. Gao and X. Li, New aspects on a low-medium temperature mechanism of $H_2$-assisted $C_3H_6$-SCR over xAg-CeZr catalyst, *Fuel*, 2021, **305**, 121574.

46 G. Xu, J. Ma, G. He, Y. Yu and H. He, An alumina-supported silver catalyst with high water tolerance for $H_2$ assisted $C_3H_6$-SCR of $NO_x$, *Appl. Catal., B*, 2017, **207**, 60–71.

47 J. Ji, X. Lu, C. Chen, M. He and H. Huang, Potassium-modulated delta-$MnO_2$ as robust catalysts for formaldehyde oxidation at room temperature, *Appl. Catal., B*, 2020, **260**, 118210.

48 L. Q. Nguyen, C. Salim and H. Hinode, Roles of nano-sized Au in the reduction of $NO_x$ by propene over $Au/TiO_2$: an in situ DRIFTS study, *Appl. Catal., B*, 2010, **96**(3–4), 299–306.

49 K. Shimizu, J. Shibata, H. Yoshida, A. Satsuma and T. Hattori, Silver-alumina catalysts for selective reduction of NO by higher hydrocarbons: structure of active sites and reaction mechanism, *Appl. Catal., B*, 2001, **30**(1–2), 151–162.

50 K. Shimizu, J. Shibata, A. Satsuma and T. Hattori, Mechanistic causes of the hydrocarbon effect on the activity of $Ag-Al_2O_3$ catalyst for the selective reduction of NO, *Phys. Chem. Chem. Phys.*, 2001, **3**(5), 880–884.

51 K. Shimizu, H. Kawabata, A. Satsuma and T. Hattori, Role of acetate and nitrates in the selective catalytic reduction of NO by propene over alumina catalyst as investigated by FTIR, *J. Phys. Chem. B*, 1999, **103**(25), 5240–5245.

52 J. Li, R. Ke, W. Li and J. Hao, Mechanism of selective catalytic reduction of NO over $Ag/Al_2O_3$ with the aid of non-thermal plasma, *Catal. Today*, 2008, **139**(1–2), 49–58.